An Asymmetric Star Design for the Dynamic Control of Quantum-Emitter-Coupled Plasmonic Nanoantenna Emission

Hisham A. Amer[1], Tamer A. Ali [2,3], Ashraf H. Badawi[2]
[1] University of Science and Technology-Zewail City, Physics Program, Giza, Egypt, s-hisham.amer@zewailcity.edu.eg,
[2] University of Science and Technology-Zewail City, Communications and Information Engineering Program, Egypt, abadawi@zewailcity.edu.eg
[3] Department of Engineering Mathematics and Physics, Faculty of Engineering, Cairo University, Giza, Egypt, tali@zewailcity.edu.eg

***Abstract*— Plasmonic single nanoantennas and meta-surfaces can both enhance and manipulate emission from potential quantum emitters while their layer-like nano thick structure renders them integrable into quantum and nano-devices. Here we proposed an Asymmetric Star Nanoantenna design, which when coupled to a single quantum dot emitter, offered unique resonant enhancements in both single and array arrangements. This enhancement was most established with the array, where 3 main polarization tunable behavioral states were identified, ones we described as double, single and steady mode patterns. This polarization driven functionality could offer a much-needed means of control over quantum emitters.**

***Index Terms*— *nano*antennas, plasmonic metasurface, plasmonic arrays, quantum emitter, quantum-dot plasmon coupling, polarization dependent tuning, COMSOL.**

I. Introduction

With the rise of quantum information, the need for more compact and efficient means of controlling light has risen as well. One such tool, lies in plasmonic nanostructures, which have shown promise in controlling the spontaneous emission of quantum dots, among other sources, through coupled antenna configurations to manipulate light at the nanometer scale. Furthermore, there's been special interest in dynamically tunable responses, as they offer greater utility in nanophotonics applications. The most common approaches to dynamic control, beyond directly adjusting the structural parameters, are through mechanical stress, gate voltage control, thermal stress and magnetic field manipulation [1]–[5]. These methods however have yet to offer the range, versatility or practicality needed. In this study, we introduce a relatively straightforward structural means of control, using a newly proposed asymmetric star nanoantenna design. The proposed design, whether as an array or a singular unit, could offer control within visible light frequencies through a selection of polarization dependent behavioral patterns.

II. Materials and Methods

A. Selecting appropriate investigation tools and parameters

First, to investigate the coupling behavior of the quantum dot (QD) excitation source, it was our goal to utilize a relatively simple, as far as setup is concerned, yet computationally demanding approach, as opposed to a more exact, yet often too abstract analytical approach. One such route was full dependence on finite element analyses and simulations to model the physical interactions. Accordingly, the COMSOL Multiphysics v5.3 software was used to reproduce previous experimentally verified results from various resonance coupling studies[3], [6]–[10] both for single and array gold nanoantenna arrangements. Preliminary testing yielded comparable resonance peaks, in both shape and frequency, ranging from 650-850 nm based on geometry and study setting in addition to outputting familiar Electric-field patterns as shown in Fig. 1. Accordingly venturing further with new modifications was justifiable.

Mostly influenced by the studies depicting a QD emitter coupling to nanorods [6], [8], a largely similar setup was adopted for all simulations. The unit cell's (320 nm x 250 nm) base was that of a 100 nm thick GaAs semiconductor substrate, and assigned a frequency independent relative primitivity of 12, as per COMSOL built in material library. It was in turn covered by a native 2 nm thick Ga2O3 layer with a frequency independent relative primitivity of 4. This was in turn evenly coated with another passive 3 nm thick Al2O3 layer with a relative primitivity of 3.14. Finally, the Gold nanoantenna's underside was padded by an adhesive oxidized chromium layer with relative permittivity -1.8.

Gold on the other hand attributes being most sensitive to the visible and near infrared wavelengths to its highly negative real part and significant imaginary part of the relative permittivity at these frequencies. It was therefore modelled with both complex and real parts. Values for gold were interpolated from a recent database for 20-200 nm thin gold films published by Yakubovsky et al. [11].

B. Changes to typical nanoantenna resonance study design, simulation process and evaluation methods.

A key difference in the study from those referenced was the omittance of the pseudo-analytical nature of utilizing the Lorentz reciprocity theorem [8], [12] to calculate an analytical incident field intensity from QD dipoles for a scatter field study. Instead, a fully simulated field approach was taken, where the QD was modelled as an electric point

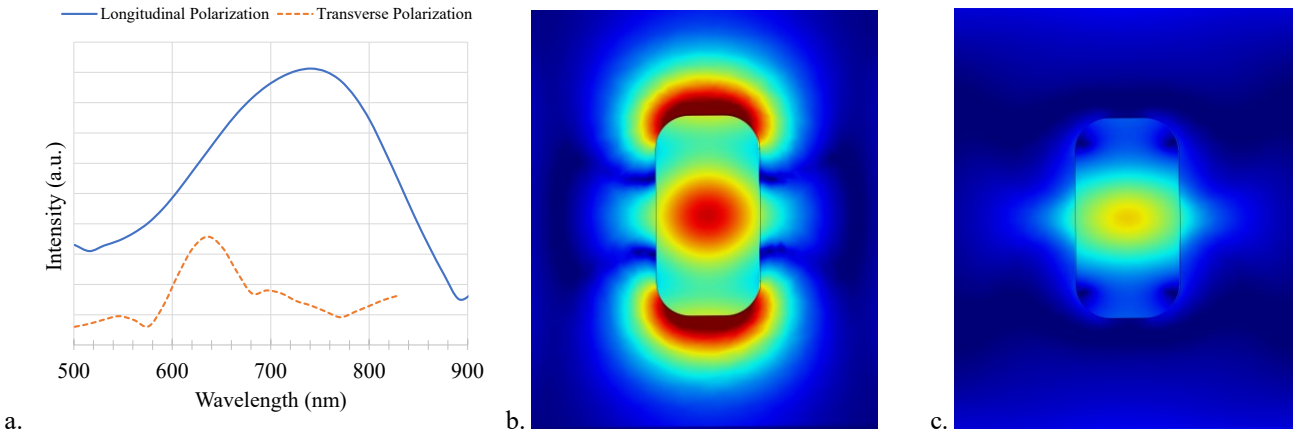

Figure 1. (a) Results from the verification phase where a rod shaped nanoantenna cell was used to test the the proposed methodology. The graph clearly shows both familiar peak position and shape which were consistent with previous cited studies. This emission peak is an indication of the coupling of gold nanoantennas to the excitation source within the visible light range. **(b)** Response of the nanoantenna to longitudinally polarized excitation source at 742 nm. **(c)** Weaker response of the nanoantenna to longitudinal polarized source at 900 nm as depicted by the first graph.

dipole and the resulting interaction was directly studied from the simulation on a full field basis. To do that, the QD would be placed 23 nm below the undersurface of the gold nanoantenna, embedded in the GaAs crystal substrate, and it would freely interact with the surrounding. Accordingly, field calculations were done on a two-step basis to deduce the resonance response of the nanoantennas. First the full field with the antenna set to air was evaluated, then another full field simulation followed with antenna set to gold. The response of gold was to be evaluated by obtaining the difference between the two cases in terms of their maximum field values along each of X, Y and Z coordinates separately, where the norm of this resultant vector would be taken to be proportional to the scattered field intensity.

C. Setting up a unique Asymmetric Nanoantenna design, and expected outcomes.

After comparing plasmonic resonance data with those from other setups and validating that the proposed computational method could simulate gold's resonance coupling, an asymmetric geometry was given to the gold nanoantenna. Fig. 2 shows the overall view of the asymmetric design and meshing. The arms were assigned long, intermediate and short lengths, 135 nm, 70 nm and 45 nm respectively and a width of 25 nm.

The QD was placed 23 nm below the antenna undersurface nearest to the center of mass of the asymmetric star geometry. It was predicted that the direction of QD dipole polarization would interact and resonate uniquely with the asymmetric geometry at polarization angles, most notably along and perpendicular to the arms. The hypothesis was that the resulting plasmonic resonance behavior, in terms of field intensity peaks' magnitudes and form, could be controlled to some practical degree in a way that was not possible with a typical single nanoantenna rod design. Accordingly, the behavior of a single versus an array of asymmetric stars was also found worth investigating. To minimize propagation of errors, in an attempt to overcome dependence on simulation with no analytical input, an extra fine meshing was utilized for the simulation down to 0.1 nm in certain areas.

Simulations were done for both single nano-antennas with a cuboidal perfectly matched layer at the boundaries of the single cell, and for an array of nanoantennas each with their own QD excitation source, with floquet periodic boundary conditions. A parametric sweep ran from 450-900 nm emissions, to capture most of the visible range over 6 key polarization angles.

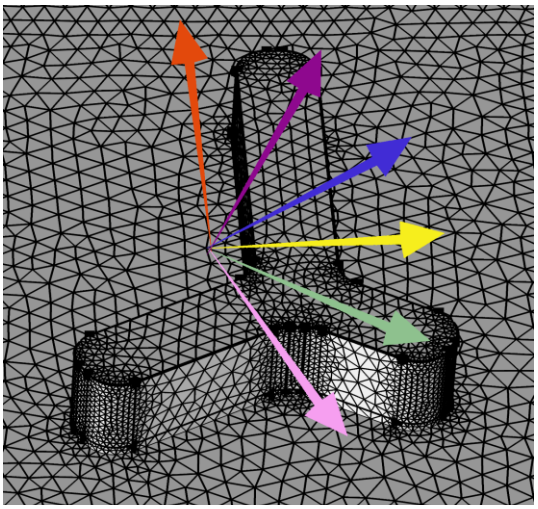

Figure 2. The extra fine mesh of the proposed Asymmetric star design; the long 135 nm arm at 0-degrees (amber arrow); the direction normal to the short arm at 30 degrees (violet); the direction along the intermediate 70 nm arm at 60 degrees (blue); the direction normal to the longest arm at 90 degrees (yellow); the direction along the short 45 nm arm at 120 degrees(green); a direction normal to the intermediate arm at 150 degrees (mauve). The color codes that will be used in the legends later.

III. Results and Discussion

Data from the parametric sweeps across the 450-800 wavelength range was plotted for both single cell and array arrangements of nanoantennas. Results are summarized in shared graphs in Fig. 3 and 4.

A. Single cell nanoantenna arrangment

First, the single nanoantenna simulation results- Fig. 3a, show three resonance peaks for each of the 90 degrees and 120 degrees polarizations. The emission peaks seem less sharp for the 60 degrees graph and practically absent for the 0 degrees case within our specified range. For a more detailed assessment, mean values and standard deviations were calculated for peak regions which lay within the 650-900 nm interval. The non-zero angles showed peaks (in arbitrary units (a.u.) maxed at 5.00) of 4.14, 4.01, 4.71, with means and standard deviations (SD) of 2.95+/- (0.79), 2.05+/-(0.98) and 2.75+/- (1.09), for 60, 90, and 120 degrees polarizations respectively. In contrast, the 0 degrees case had a maximum value of 3.25 with 2.80+/- (0.47) mean and SD, by far the lowest, that's more than 2.3 times the spread of the largest peak.

It was clear that the positions of the peaks were fixed at 711 nm, 600 nm and 515 nm, (+/- 15 nm given the resolution of 15 nm step in the sweep) regardless of polarization angle at least for angles between 60 and 120. The general trend was towards larger angles showing sharper and higher peaks. Accordingly, below 60 degrees and most notably at 0 degrees, widening of the spectrum was sufficient to force peaks to coalesce, essentially erasing the ones that did within our frequency range. The resulting regions coalesced into a single plateau with a SD falling down to less than half of that of the largest peak.

Despite the 0 degrees case being flatter than its counterparts, it had spread itself into a new region of maximum emission at the 650 nm region, that's still a significant shift in plasmonic resonance. It also provides a steady damped region of up to 0.47 a.u. standard deviation from effective coupling around the 600-800 nm range, maintaining a level of consistency that is in stark contrast to the sharp 700 nm sharp peaks for larger polarization angles.

B. Nanoantenna array arrangment

Second, the nanoantenna array simulation results, shown in Fig. 3b, take this polarization sensitive damping effect a step further. The three peaks are no longer identifiable for any angle, instead, the 60 degrees and 120 degrees polarizations show 2 clear relatively wider peaks around both the 700nm and 500 nm marks. Despite this, the 90 degrees polarization seems to lose any effective peak throughout the 550-800 range, and offers steady damped emission in the same region. In addition, it gives a clear peak, comparable to the 120 degrees and 60 degrees, below the 580 nm mark. By

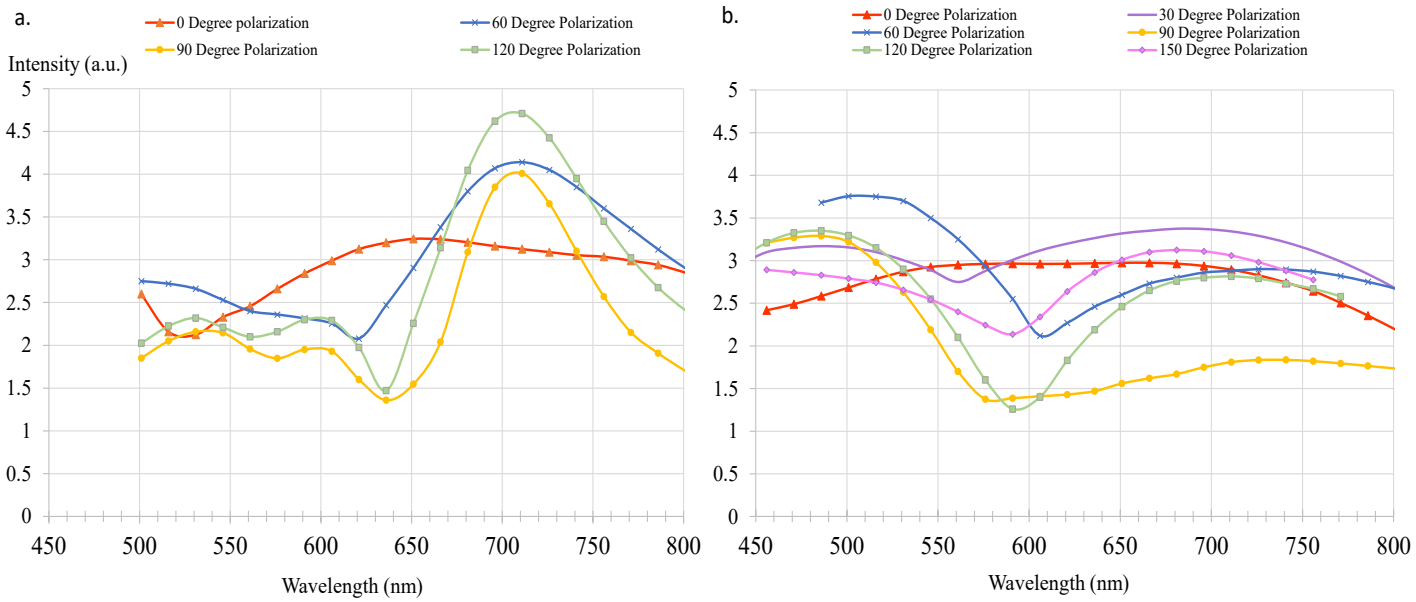

Figure 3. (a) 4 different electric dipole polarization angles and the resulting intensities *, in arbitrary units (au), from a single asymmetric gold nanoantenna setup. Three resonance peaks are clearly shown for each of the 90 and 120 degrees, less so for the 0-degree and 60-degree cases. **(b)** 6 different electric dipole polarization angles and resulting intensities from an array of asymmetric gold nanoantenna. Three resonance peaks have vanished for the 90 and 120 nm nanoantennas and have been replaced by 2 main broader flatter peaks. The smaller degrees are start to give off zones of near constant coupling.

* intensity axes in both a. and b. are of the same scale in the same arbitrary units, they essentially share the axis.

a similar token, the angles 30 and zero have flattened to the degree that they no longer exhibit peaks, especially the 0-degree polarization. They offer steady emission through the 550-800 nm range but as unlike the 90-degree case, they do so at a much higher intensity and through a wider range.

To analyze this further, the 3 main checkpoints of the polarization driven behavioral patterns, emphasized in Fig. 4, are identified and broken down further. The first pattern being one with a two-peak response, which is to be discussed through the 120 degrees case. This pattern can in turn be reduced to a single peak lying directly next to a steady emission region, which introduces the second pattern to be discussed through the 90 degrees case. The third and final pattern is observed at the lowest angles, where damping forces peaks to fuse into a constant region, similar to what was seen in the 0 degrees case for the single antenna, but to a much more significant extent, this is most clear with the 0 degrees polarization as expected.

i. The First "two peak mode" Pattern :

In the first pattern, we observe peaks for the array of asymmetric nanoantennas happening roughly around the 700 and 500 nm marks. They are relatively wider and less sharp than their single antenna counterparts. the 500 nm peak is sharper, having an SD of 0.75 a.u. which is close to 1.3 times that of its single asymmetric antenna counterpart, and comparable to the 0.5 a.u. seen with single rods investigated in the testing phase of this study, like the rod in Fig. 1. Furthermore, the first pattern offers access to a second resonance mode, around the 700 nm mark. The second mode for the specific case of the 120 degrees polarization, was shown to be flatter, with a SD of 0.15, which is a fifth of that of the 500 nm peak. Ultimately, it unlocks two different excitation frequencies at the 500 and 700 nm wavelength marks, with similar averages 2.39 and 2.65 a.u. and comparable maxima at 3.35 and 2.82 respectively. This behavior is observed in the off 90 and off 0 degrees polarizations, so between 30 to 60 and 120 to 150. The pattern acts like two single rods at different modes, which would be activatable through polarization tuning.

ii. The Second "one peak one mode Pattern :

This pattern arises around the unique 90 degrees polarization. It maintains the peak with a practically matching intensity and SD, as it basically traces out the 120 degrees polarization behavior around the 500 nm mark. The uniqueness of this mode lies in the second 700 peak which it suppresses. By damping this peak, it creates a near steady emission region most notably between 580-800 nm, while having a relatively low mean emission at 1.75 a.u., which is half that of the peak's maximum at 500 nm. The SD being 0.09, makes it 8.33 times more spread out than at its peak.

iii. The Third "Single Steady mode" Pattern :

This pattern being similar to the 0 degrees pattern of the single nanoantenna has already been discussed, however, it provides a much more stable environment and over a longer

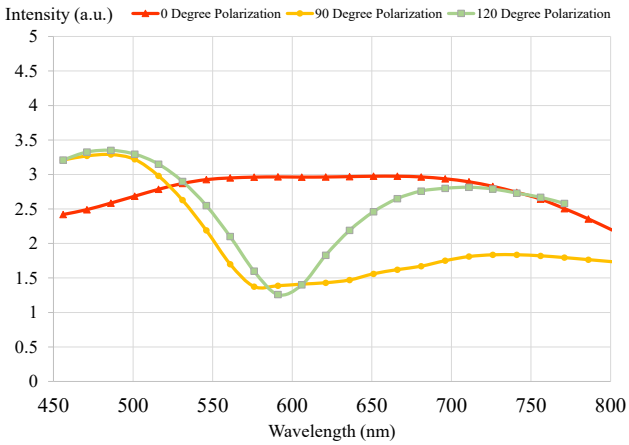

Figure 4. The 3 main modes encompassing the full range of unique array response to polarization change. Two clear peaks at 700 nm and 485 seen for the 120 degrees polarization, Damping of the 700 nm peak at 90 degrees polarization and the steady 550-700 nm mode at 0 degrees

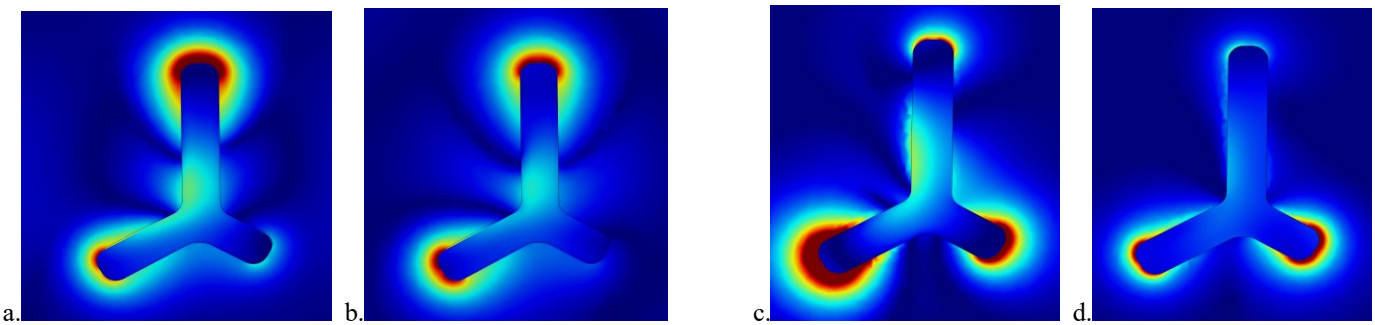

Figure 5. Response of a 0 degrees polarized excitation source around the 550 nm mark **(a)** and around the 700 nm mark **(b)** showing a clear shift in emission from the long arm pointing up, to the left arm. A mechanism that could be responsible for maintaining the steady level of emission. A contrasting behavior is seen with the response of a peak mode containing pattern, (pattern 1 or 2 discussed on the previous page). In this case **(c)** represents the re-emission at a peak frequency from a 90 degrees polarized source at 500 nm, this is a pattern 2 case, with 1 peak at 500 and a plateau of steady re-emission around the 600-800 mark. **(d)** clearly shows the damping of emission at the 800 nm mark relative to the peak at 500 nm.

interval. This single mode gives rise to a region extending from 450 to 800 nm with a mean and SD of 2.77+/- (0.234) a.u., the SD being 1.5 times more for its single asymmetric antenna counterpart. More specifically, a unique region exists from 550-700 nm which offers a mean of 2.96+/- (0.0154). This makes it around 21 times more reliable than its single antenna counterpart as a steady mode.

This unique polarization dependent response pattern, once adjusted to some operational requirements, could provide a way to focus nanoantenna enhancement and coupling to certain localized excitation frequencies by simply selecting out certain polarizations to enhance. The proposed advantage of using the asymmetric star design, is that there are a variety of different patterns with which the coupling can be expressed, introducing new "modes" that were unavailable to either rod shapes, symmetric shapes, or even single cells of the same proposed design. We've simulated how different responses can be manipulated towards certain peak frequencies or in contrast, be used to flatten the response to a near constant level for all possible excitation frequencies within some specified range under a given polarization. This could also mean that this design can offer a controlled damping mechanism for excluding random shifts in polarization from excitation sources, through coupling a plasmonic metasurface to a certain frequency that would exclude certain target polarization range; for example choosing a frequency above 600, that would exclude 90 degrees polarized rays from effective coupling with the asymmetric nanoantenna array. This includes single photon emitters whose polarizations might experience jumps in emittance, this might also provide some means of overcoming other slight fabrication discrepancies or source positioning.

Finally, it would be worth emphasizing that through monitoring the response of the different arms in different patterns of emission, the polarizations which experienced steady modes and damping, achieved this only when different antenna arms exchanged emission roles as the simulation swept through frequencies, that way the emission peaks "intersected" and coalesced, giving rise to wider regions of emission enhancement and higher averages, but lower maximum peaks levels. Through this interaction, an emission plateau could be maintained over a longer frequency range as the resonating modes of different arms intersected favorably to do so. In contrast, peak patterns, showed universal increase in emission from one or two sometimes 3 arms simultaneously.

IV. Conclusion

The simulations seem to shows a unique advantage of the asymmetric nano-star design over conventional, symmetric spheres or rods. This is especially emphasized in arrays, where it was demonstrated that by choosing a certain polarization, the same arrangement could offer one of three broad behavioral patterns in addition to controlling a gradual transition between them. These levels were either 1-The raising 2 wide peaks at the extremities of visible ranges; 2-Tuning out one of those 2 peaks in favor of a near steady damped region of relatively low intensity while offering access to either region based on operational frequencies; or 3- An overall damping of peaks in favor of an emission plateau at higher intensities. Further studies would be needed to test the practicality of such a design, and the feasibility of others and the various control patterns they might introduce.

References

[1] B. Liu, C. Tang, J. Chen, M. Zhu, M. Pei, and X. Zhu, "Electrically tunable fano resonance from the coupling between interband transition in monolayer graphene and magnetic dipole in metamaterials," *Sci. Rep.*, vol. 7, no. 1, pp. 1–8, 2017.

[2] V. Amendola, R. Pilot, M. Frasconi, O. M. Maragò, and M. A. Iatì, "Surface plasmon resonance in gold nanoparticles: A review," *J. Phys. Condens. Matter*, vol. 29, no. 20, 2017.

[3] W. S. Chang *et al.*, "Tuning the acoustic frequency of a gold nanodisk through its adhesion layer," *Nat. Commun.*, vol. 6, no. May, pp. 1–8, 2015.

[4] O. Scholder, "Fabrication , Simulation and Characterization of Tunable Plasmonic Nano Antennas .," Doctoral Theis, Dep. of Inform.Technol. Electrical Eng, ETH Zurich, 2014.

[5] F. Monticone and A. Al, "Metamaterials and plasmonics : From nanoparticles to nanoantenna arrays , metasurfaces , and metamaterials ∗," *Chinese Phys. B*, vol. 23, no. 4, 2014.

[6] M. Pfeiffer *et al.*, "Coupling a single solid-state quantum emitter to an array of resonant plasmonic antennas," *Sci. Rep.*, vol. 8, no. 1, pp. 6–11, 2018.

[7] P. K. Ghosh, D. T. Debu, D. A. French, and J. B. Herzog, "Calculated thickness dependent plasmonic properties of gold nanobars in the visible to near-infrared light regime," *PLoS One*, vol. 12, no. 5, pp. 1–11, 2017.

[8] M. Pfeiffer *et al.*, "Eleven nanometer alignment precision of a plasmonic nanoantenna with a self-assembled GaAs quantum dot," *Nano Lett.*, vol. 14, no. 1, pp. 197–201, 2014.

[9] A. G. Curto, "Unidirectional Emission of a Quantum Dot Coupled to a Nanoantenna Unidirectional Emission of a Quantum Dot Coupled to a Nanoantenna," *Science (80-.).*, vol. 329–5994, no. August, pp. 930–933, 2010.

[10] A. M. Funston, C. Novo, T. J. Davis, and P. Mulvaney, "Plasmon coupling of gold nanorods at short distances and in different geometries," *Nano Lett.*, vol. 9, no. 4, pp. 1651–1658, 2009.

[11] D. I. Yakubovsky, A. V. Arsenin, Y. V. Stebunov, D. Y. Fedyanin, and V. S. Volkov, "Optical constants and structural properties of thin gold films," *Opt. Express*, vol. 25, no. 21, p. 25574, 2017.

[12] R. Carminati, M. Nieto-Vesperinas, and J.-J. Greffet, "Reciprocity of evanescent electromagnetic waves," *J. Opt. Soc. Am. A*, vol. 15, no. 3, p. 706, 1998.